JOURNAL OF SOLID STATE CHEMISTRY 27, 71–85 (1979)

The Jahn–Teller Effect in Solid State Chemistry of Transition Metal Compounds

D. REINEN

Fachbereich Chemie der Philipps-Universität, Lahnberge, GFR–3550 Marburg/Lahn, Germany

Received May 30, 1978

The general features of the local and cooperative Jahn–Teller effect of d^n cations with E_g ground states in octahedral coordination and simple model structures are discussed. Examples of different cooperative Jahn–Teller ordering patterns and of phase transitions from static to partially dynamic and finally fully dynamic Jahn–Teller determined structures are given. While in general a tetragonally elongated coordination of the Jahn–Teller ions is favored, the compressed configuration may be stabilized under certain conditions also. It is demonstrated by some examples that the extent of the Jahn–Teller distortion depends on the symmetry and connection pattern of the polyhedra in the host lattice structure. Finally it is shown that the crossover between high- and low-spin configurations of d^7 cations is strongly influenced by the additional Jahn–Teller stabilization of the low-spin ^2E_g state.

1. Introduction

The Jahn–Teller theorem states that orbitally degenerate ground states are not possible in nonlinear systems (*1*). There will always be a normal coordinate in the point group of the complex or molecule, which provides a mechanism for reducing the symmetry, i.e., for distorting the molecule. In this way the degeneracy of the ground state is lifted and a new nondegenerate ground level is generated, which has a lower energy than the original one. Paramagnetic transition metal complexes and compounds provide ideal systems for studying the energetic and stereochemical consequences of the Jahn–Teller effect, because many d^n configurations lead to threefold and twofold orbital ground-state degeneracies in cubic coordination (Table I). Especially large level splittings are expected, if the ground state is σ antibonding. This is demonstrated by Fig. 1, where the spectroscopic and structural results of FeF_2 and CuF_2—both with rutile-type structures—are compared. The extent of the tetragonal compression of the FeF_6 octahedra and the splitting of the π-antibonding T_{2g} ground state is less distinct than the tetragonal elongation of the CuF_6

TABLE I

GROUND STATES OF d^n CATIONS IN CUBIC COORDINATION[a]

octahedral		
$E(^2\Theta)$	$d^4, d^9, \underline{d^7}$	$Cr^{2+}, Mn^{3+}; Cu^{2+}, Ag^{2+}; Co^{2+}, Ni^{3+}$
T_1 $(^4\Pi)$	$d^2, d^7, \underline{d^4}$	$V^{3+}; Co^{2+}$
T_2	$d^1, d^6, \underline{d^5}$	$Ti^{3+}, V^{4+}, Cr^{5+}; Fe^{2+}$
tetrahedral		
$E(^4\Pi)$	$d^1, d^6,$	
T_1 $(^2\Theta+^4\Pi)$	$d^3, d^8,$	Ni^{2+}
T_2	$d^4, d^9,$	Cu^{2+}

[a] Low-spin configurations are underlined.

0022-4596/79/010071-15$02.00/0

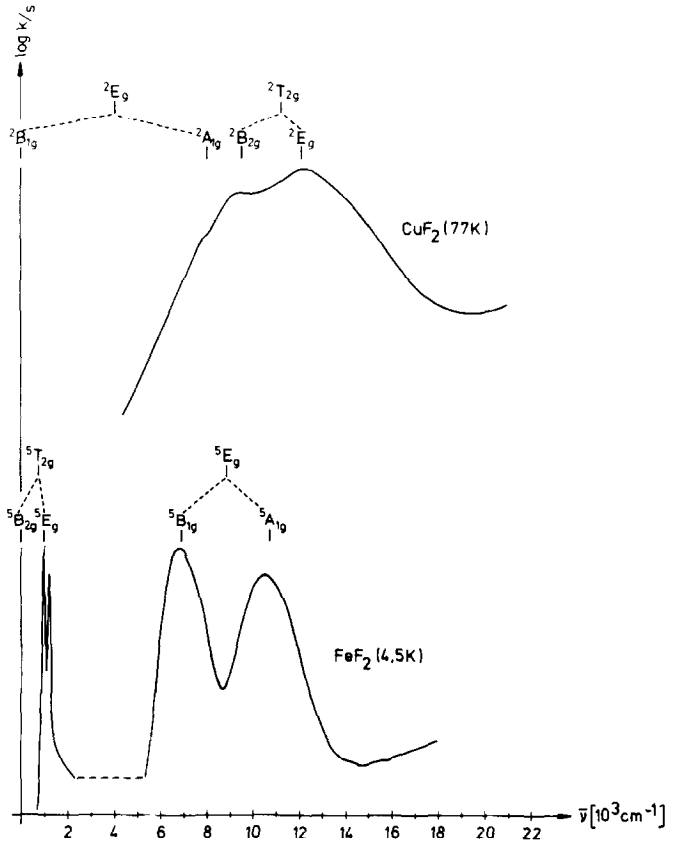

FIG. 1. Ligand field spectra and band assignments (O_h and D_{4h} symmetries) of Cu^{2+} and Fe^{2+} in octahedral F^- coordination. [The splittings of the T_{2g} ($3\delta_2$) and E_g levels ($4\delta_1$), the octahedral ligand field parameter Δ, as well as the Cu–F and Fe–F bond lengths in CuF_2 and FeF_2 are also given.] Note: The $^5B_{2g} \rightarrow {}^5E_g$ transition in FeF_2 is found by electronic Raman spectroscopy (*2*).

octahedra and the splitting of the σ-antibonding E_g ground state. The extent of the Jahn–Teller effect decreases, if the coordination is changed from octahedral to tetrahedral. The lower Δ values in the case of tetrahedral coordination are equivalent to a weaker coupling of the *d* electrons to the ligand environment and induce smaller ground-state splittings and less distinct distortion effects of the transition metal tetrahedra (Fig. 2). The following discussion will be restricted to E_g ground states in octahedral coordination exclusively. The only vibrational mode in the O_h-point group, which can be active in removing the degeneracy of an electronic E_g state, is of E_g symmetry also. The linear coupling between electronic and vibrational motions of these symmetries leads to a potential surface, which is called the "mexican hat" (Fig. 3a). The ring-like minimum positions of the lower potential curve correspond to the lower split level of the E_g ground state, while the vertical transition from this ring to the upper potential surface gives the energy of the first transition in the ligand field spectrum of CuF_2 (Fig. 1). The positions on the ring of minimum energy are defined by the radial coordinate ρ—measuring the extent of the distortion of the octahedra—and by the angular parameter φ, which describes the symmetry of distortion. The distortion geometry may be of Q_θ or Q_ε symmetry or correspond to any linear combination between Q_θ and Q_ε. Taking

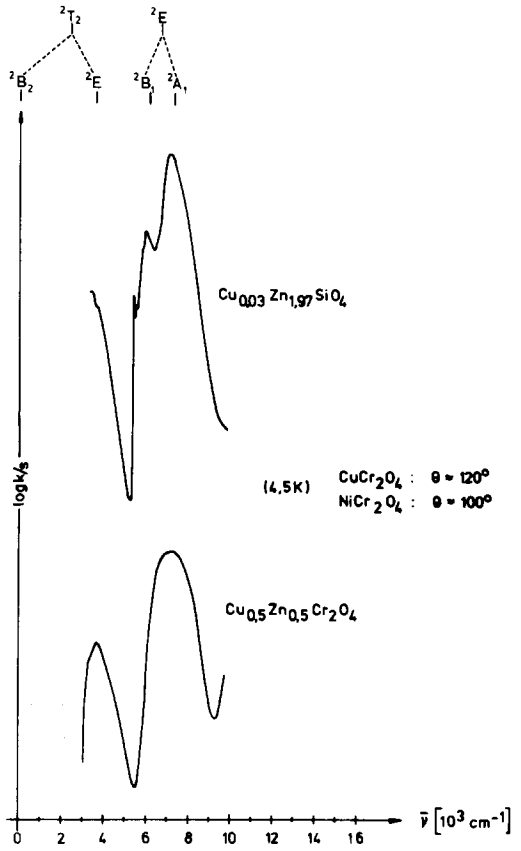

FIG. 2. Ligand field spectra of Cu^{2+} in tetrahedral coordination of oxygen (phenacite and spinel) host lattices; $3\delta_2 \simeq 3600\ cm^{-1}$, $4\delta_1 \simeq 1200\ cm^{-1}$.

nonlinear coupling terms between electronic and vibrational motions into account, the lower potential surface is slightly modified by an additional warping, however (Fig. 3b). The three additional minima at $\varphi = 0$, 120, and 240° represent tetragonal elongations of the octahedra along the x-, y-, and z-axes, respectively. These three "conformations" can be transformed into each other by rotations around a threefold axis. The three minima are separated by saddlepoints at $\varphi =$ 180, 300, and 60°, positions which characterize tetragonally compressed octahedra. All other φ values correspond to orthorhombic distortions of the octahedra (*3*). This description takes into account the experimental result that the tetragonal elongation is energetically slightly favored with respect to the compressed configuration for d^4, d^9, and low-spin d^7 cations. Indeed, in all cases, in which Cu^{2+} or low-spin Co^{2+} is isomorphously substituted into an *octahedral site of regular O_h symmetry*, the induced distortion geometry is elongated in nature—very frequently superimposed by a small orthorhombic component, however.

2. The Local and Cooperative Jahn–Teller Effect

The basic features of the local Jahn–Teller effect will be discussed now, taking mixed crystals $Ba_2Zn_{1-x}Cu_xWO_6$ as a typical example. The cubic host lattice Ba_2ZnWO_6 crystallizes in the ordered perovskite or elpasolite structure (Fig. 4). This lattice consists of a three-dimensional array of octahedra, which are linearly linked with each other by common corners. The octahedral sites are alternately occupied by the Zn^{2+} and W^{6+} ions, while the Ba^{2+} ions are 12-coordinated by the oxygen ligands. If Cu^2 ions are doped into the Zn^{2+} site, an anisotropic EPR powder spectrum is obtained at low temperatures, which indicates statically distorted CuO_6 octahedra with the geometry of a tetragonal elongation. Raising the temperature transforms the statical deformation into a dynamical one (*4*). kT has become comparable to the energy barrier between the minima in the lower potential surface. The long axis of each of the elongated octahedra changes between the x-, y-, and z-directions—with a frequency which is fast with respect to the time scale of EPR spectroscopy. This means that the octahedra are regular in time average at high temperature. The ligand field spectra reflect the symmetry of tetragonally distorted CuO_6 octahedra however, irrespective of whether the Jahn–Teller effect is static or dynamic in nature (Fig. 5).

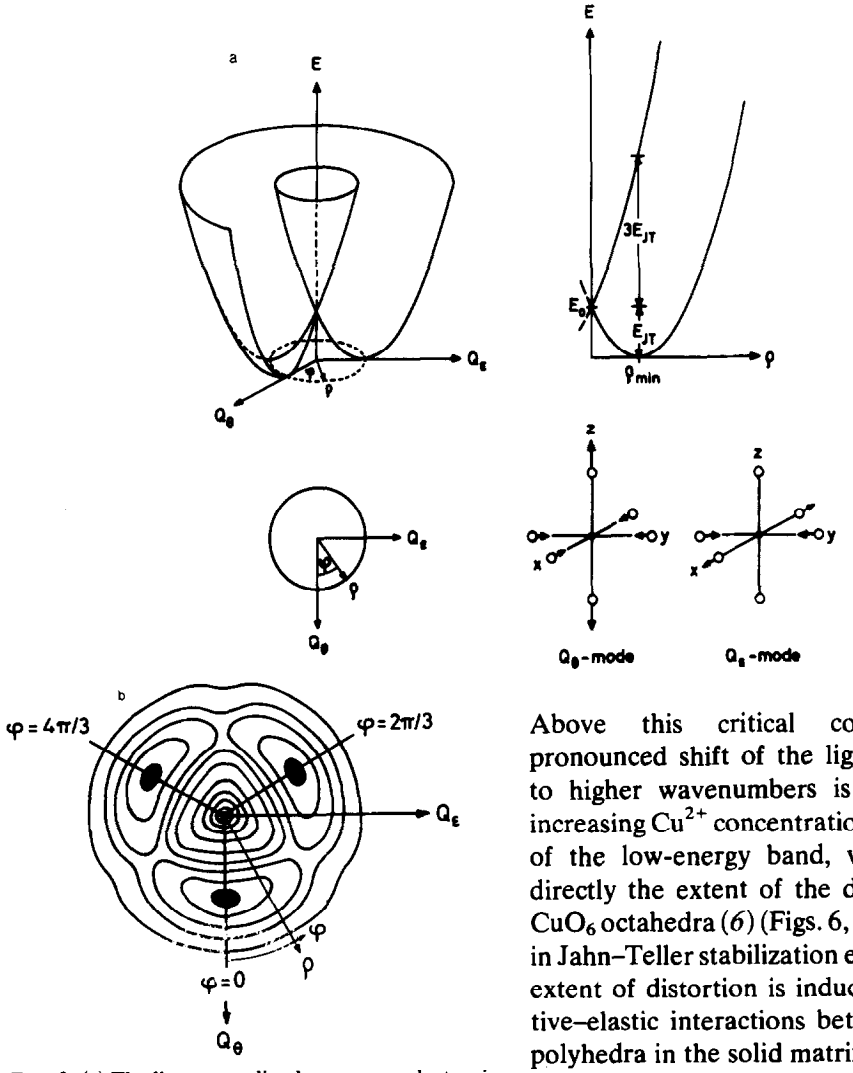

FIG. 3. (a) The linear coupling between an electronic E_g level and a vibrational E_g mode (components: Q_θ, Q_ε) ($4E_{JT} \equiv 4\delta_1$). (b) The influence of nonlinear coupling terms on the lower potential curve.

If the concentration of Jahn–Teller unstable cations in the solid matrix increases, however, coperative–elastic interactions between the Jahn–Teller centers must be allowed for in addition. Figure 6 illustrates that a phase transition from the cubic host-lattice structure to a tetragonal lattice with $c/a > 1$ occurs, if the Cu^{2+} concentration is continuously raised in the mixed crystal series $Ba_2Zn_{1-x}Cu_xWO_6$ till $x = 0.23$ (*5*).

Above this critical concentration a pronounced shift of the ligand field bands to higher wavenumbers is observed with increasing Cu^{2+} concentration—in particular of the low-energy band, which measures directly the extent of the distortion of the CuO_6 octahedra (*6*) (Figs. 6, 7). This increase in Jahn–Teller stabilization energy and in the extent of distortion is induced by cooperative–elastic interactions between the CuO_6 polyhedra in the solid matrix. In addition to this energetic effect the *long axes* of these polyhedra orientate *parallel* to each other

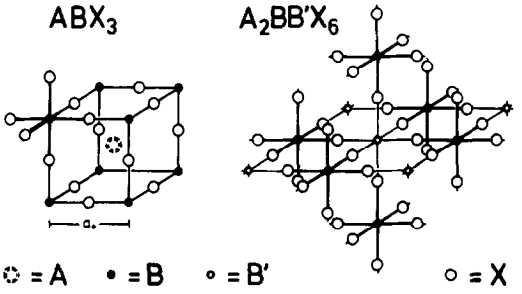

FIG. 4. The perovskite structure (*left*) and the framework of octahedra in the ordered perovskite (elpasolite) structure (*right*).

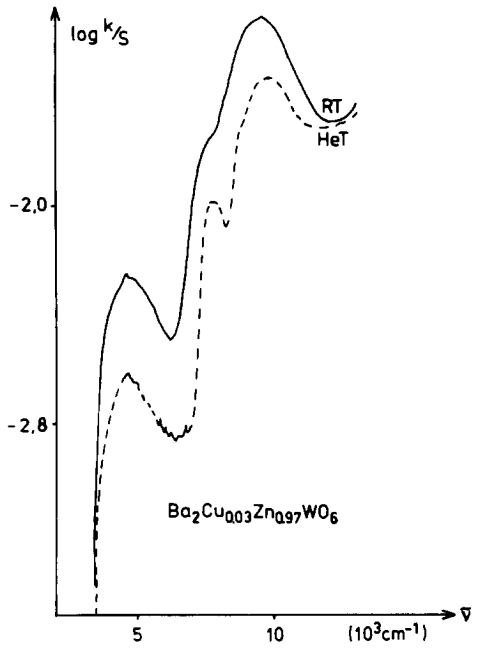

FIG. 5. Ligand field spectrum of cubic Cu^{2+}-doped Ba_2ZnWO_6.

above the critical concentration, leading to a distorted unit cell with $c/a > 1$. The symmetry of the cooperative Jahn–Teller ordering just described is called *ferrodistortive* (*7, 8*). The phase line, separating the cubic from the tetragonal modification, demonstrates that the structure with higher symmetry is favored at higher temperatures (Fig. 6).

In the perovskite structure, in which every octahedral B site (Fig. 4) may be occupied by a Jahn–Teller unstable cation, a different kind of cooperative order is observed, which is called *antiferrodistortive* and which induces a tetragonal distortion of the unit cell with $c/a < 1$ (*7, 8*). This order is best described by two ferrodistortive sublattices, the preferred long axes of which lie perpendicular to each other in the (001) planes (Fig. 8). This order is found if in fluoridic compounds of the stochiometry $A^IB^{II}F_3$ the B^{II} ion is Cu^{2+} or Cr^{2+} and may be visualized by two vectors pointing towards $\varphi \approx 120$ and 240° in the $\rho\varphi$-plane of the mexican hat (compare Fig. 3), which represent the two ferrodistortive sublattices. The resultant vector points toward $\varphi = 180°$ and describes the tetragonal compression of the unit cell.

An interesting class of compounds with respect to cooperative Jahn–Teller effects is the nitrocomplexes $A^I_2NiB^{II}(NO_2)_6$ (A^I: Cs, Rb, Tl, K; B^{II}: Ca, Sr, Ba; Pb) with elpasolite-analogous structures. The NO_2 groups link Ni^{2+} and B^{2+} via common corners, with the nitrogen atoms bonded to the transition

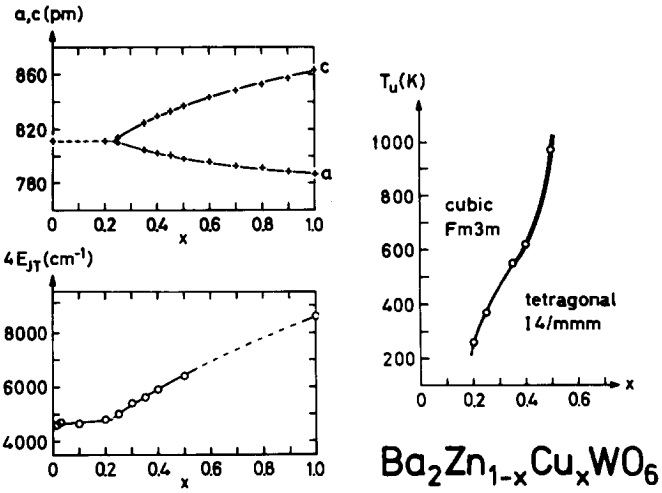

FIG. 6. Unit cell dimensions, phase line, and ^2E_g ground-state splittings for mixed crystals $Ba_2Zn_{1-x}Cu_xO_6$. (The phase transition is continuous below $x = 0.35$ and of first order at $x > 0.35$).

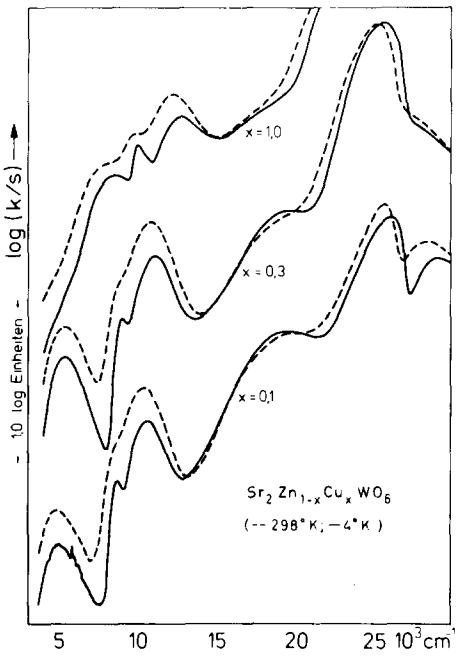

FIG 7. Ligand field spectra of mixed crystals $Sr_2Zn_{1-x}Cu_xWO_6$ (d–d transitions below 15 000 cm^{-1}).

metal ion and the B^{2+} ions coordinated by 12 oxygen atoms (*10, 11*) (Fig. 9). If Ni^{2+} is substituted by Cu^{2+} the unit cells become pseudotetragonally distorted. The axial ratio is $c/a > 1$, if B is an alkaline earth ion. The cooperative order is ferrodistortive as in the elpasolite complexes discussed previously (*13*). While the Cu^{2+} compounds remain pseudotetragonal up to their decomposition temperatures, the corresponding Co^{2+} complexes, which contain the d^7 cation in the low-spin configuration, exhibit second-order phase transitions to cubic structures at higher temperatures (*10, 14*). The statically elongated CoN_6 polyhedra undergo a transition to a dynamical distortion, as is easily deduced from the EPR spectra.

In the case of the Cu^{2+} complexes with Pb^{2+} in the B site the low-temperature γ modifications crystallize pseudotetragonally again, but with $c/a < 1$. The elongated CuN_6 octahedra exhibit an antiferrodistortive order this time (*13, 15a*). This pattern of cooperative Jahn–Teller order induces a

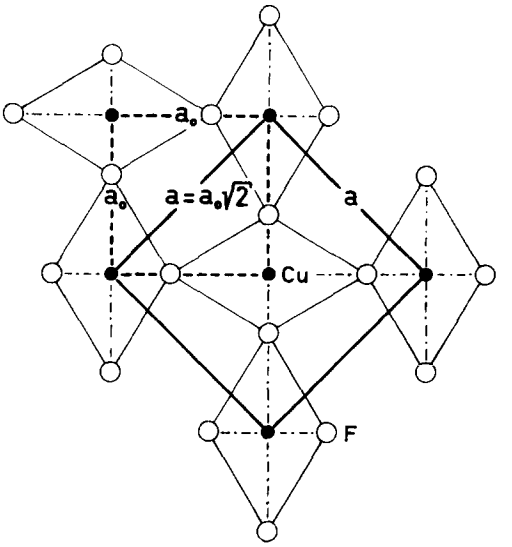

FIG. 8. Antiferrodistortive order of elongated octahedra in $KCuF_3$ (*9*) (view into the (001) planes of the tetragonal structure).

strong distortion of the B coordination in the (001) planes (Fig. 10). While the highly polarizable Pb^{2+} ion tolerates this appreciable deformation of its coordination sphere, the ionic and rigid alkaline earth ions cannot

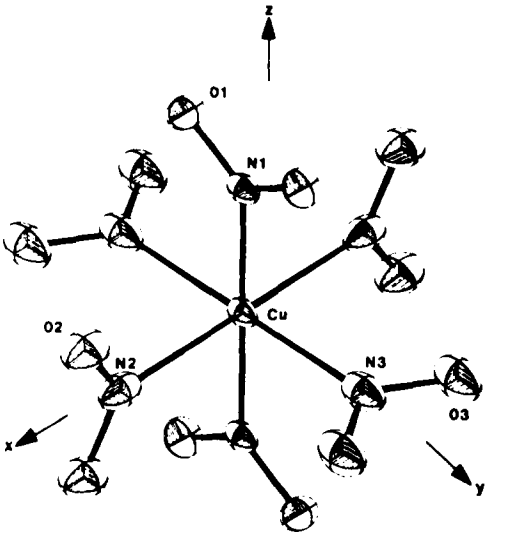

FIG. 9. The octahedral coordination of the transition metal ion by the nitrogroups in complexes $A_2^I T^{II} B^{II}(NO_2)_6$ (T^{II}: Ni, Cu, Co, Fe). [Neutron diffraction structural analysis of β-$Cs_2PbCu(NO_2)_6$ (*12*).]

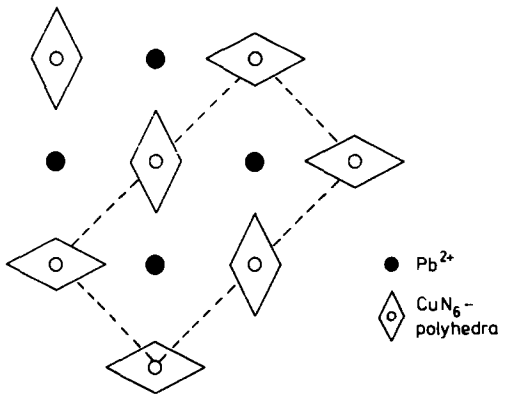

FIG. 10. Antiferrodistortive order of elongated CuN_6 octahedra in γ-$A_2^1PbCu(NO_2)_6$ (view into the (001) planes of the pseudotetragonal structure).

be stabilized in this type of cooperative order. Obviously the antiferrodistortive order is energetically slightly preferred with respect to the ferrodistortive alternative in structures with corner-connected octahedra. Additional energetic effects, however, depending on the topology of the host-lattice structure, may nevertheless stabilize the ferrodistortive order. The γ modifications show phase transitions to β structures, in which there is a dynamic equilibration of the long and short Cu–N bond lengths in the (001) planes, leading to tetragonally compressed CuN_6 octahedra in time average. This dynamical process was suggested by EPR data (*15*) and supported by neutron diffraction structure analysis (*12*). The thermal ellipsoids of the N and O atoms in the "dynamic plane" are directed with their long axes along or parallel to the CuN bonds, in contrast to the situation along the pseudotetragonal c direction (Fig. 9). The planar dynamic β modification finally transforms into the cubic high-temperature α phase, which is characterized by a three-dimensionally dynamic Jahn–Teller effect. Both phase transitions are of first order, as can be deduced from EPR spectroscopic, structural, and calorimetric measurements (*8, 15, 16*).

3. $Cu^{2+}(Cr^{2+}, Mn^{3+})$ in Tetragonally Compressed Octahedral Coordination (?)

We now proceed from the elpasolite- and perovskite-lattice to structures, in which the corner connection of the octahedra is interrupted in one dimension (Fig. 11). Layer structures of this kind—the K_2ZnF_4 and Ba_2ZnF_6 types for example—already contain slightly tetragonally compressed ZnF_6 octahedra as a consequence of purely geometric anisotropy effects. In spite of this geometric feature, which should favor a tetragonally compressed coordination for Cu^{2+} also, the compounds Ba_2CuF_6 and K_2CuF_4 contain elongated CuF_6 octahedra in antiferrodistortive order, as follows from structural (*17–19*) and spectroscopic data (*20*). If Cu^{2+} ions are incorporated into the Zn^{2+} site of Ba_2ZnF_6 in lower concentrations, however, the EPR spectra of compressed CuF_6 octahedra are observed (*21*) (Fig. 12). Angular overlap calculations

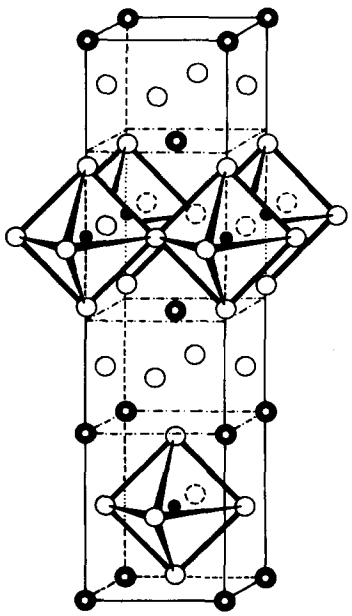

FIG. 11. The structure of Ba_2ZnF_6 (*17*).

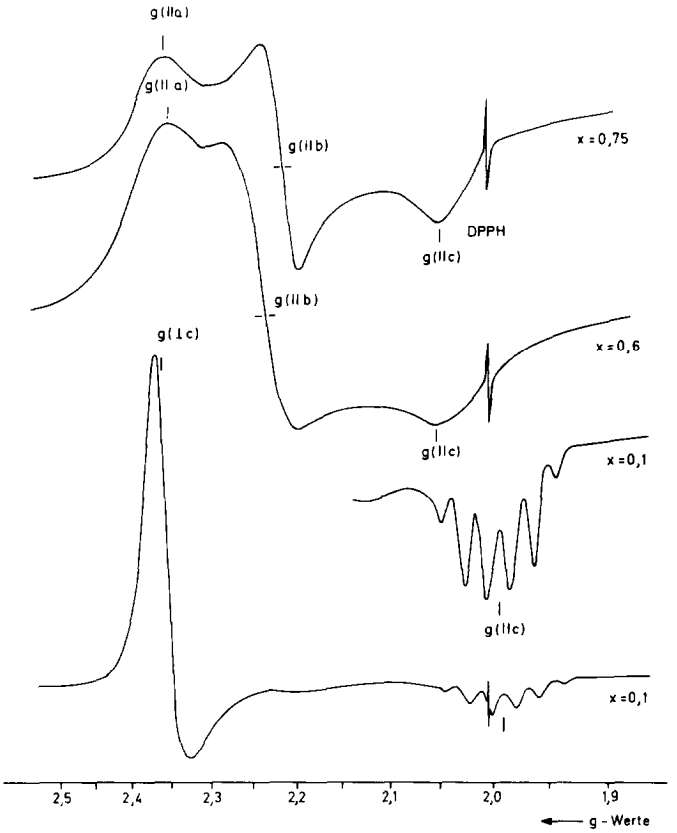

FIG. 12. EPR spectra of mixed crystals $Ba_2Zn_{1-x}Cu_xF_6$ (*21*). [$x = 0.1$: compressed CuF_6 octahedra; $g_{\parallel} \lesssim 2.00 < g_{\perp}$; $x = 0.75$: (disturbed) antiferrodistortive order of elongated octahedra.]

on the basis of the ligand field energies show that the extent of compression exceeds by far the small host-lattice effect. We can conclude that there is a true Jahn–Teller stabilization in a compressed coordination geometry. Obviously the host-lattice distortion is energetically sufficient to overcompensate the difference in Jahn–Teller stabilization energy for the compressed and the elongated coordination. Increasing x in the mixed crystal series $Ba_2Zn_{1-x}Cu_xF_6$ above 0.3, however, changes the coordination geometry from compressed to elongated. A cooperative acentric movement of the bridging fluorine ligands in the (001) planes along the CuF bond directions provides a simple mechanism by which the two alternative coordination geometries can be transformed into one another (Fig. 13). At $x \lesssim 0.3$ the potential surface of the ground state has only one minimum at $\varphi = 180°$. With increasing x the vibronic Jahn–Teller coupling becomes larger, however, and two minima symmetrical to $\varphi = 180°$ develop, separated by a flat saddlepoint at $\varphi = 180°$. Finally the two minima reach the positions $\varphi \approx 120°$ and $\varphi \approx 240°$, corresponding to the two ferrodistortive sublattices, which characterize the antiferrodistortive order of elongated CuF_6 octahedra (compare Fig. 3).

As already mentioned the same cooperative Jahn–Teller order is found in $A^{I}_2CuF_4$ (A^{I}: NH_4^+, K^+, Tl^+, Rb^+). For the corresponding Cr^{2+} chlorides a tetragonally compressed $CrCl_6$ coordination is reported, however, as the result of powder neutron

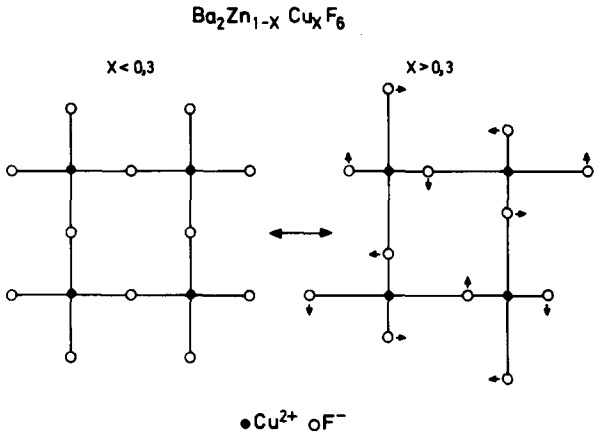

FIG. 13. The (001) planes of $Ba_2Zn_{1-x}Cu_6F_6$. [*Left:* compressed coordination; *right:* elongated CuF_6 octahedra; The arrows indicate additional movements of the F^- ligands, leading to a somewhat disturbed antiferrodistortive order (*21*).]

diffraction data (*22*). Figure 14 shows the typical result of a magnetic susceptibility measurement, indicating parallel spin–spin interactions and ferromagnetic order at low temperatures (*23*), and Fig. 15 demonstrates that there is an interesting correlation between the magnetic structure and the cooperative Jahn–Teller order. It is easily deduced from a simple superexchange model that only an antiferrodistortive order of elongated $CrCl_6$ octahedra can account for ferromagnetic interactions. The alternative picture of compressed octahedra in ferrodistortive order would unambiguously lead to antiferromagnetism. This result casts some doubt on the reported tetragonal compression of the $CrCl_6$ octahedra in these compounds. The same antiferrodistortive order may be suggested for compounds of stochiometry A^IMnF_4, which again contain corner-connected MnF_6 polyhedra in two dimensions. Like the Cr^{2+} compounds just

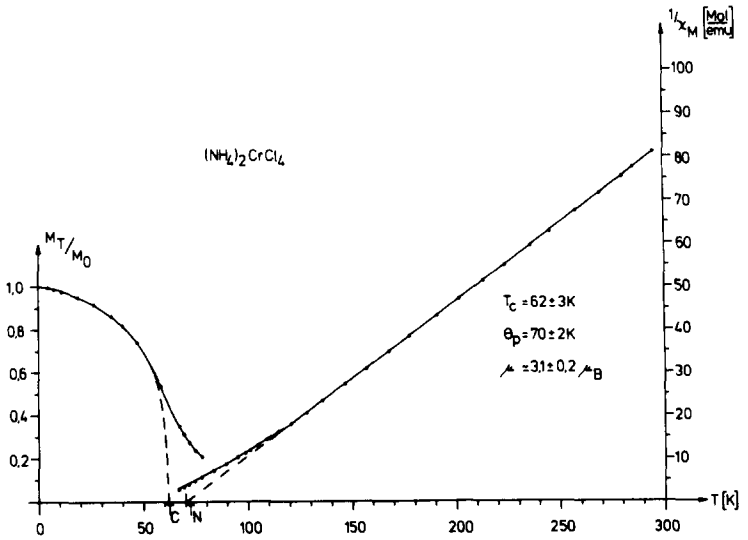

FIG. 14. Magnetic susceptibility and magnetization data for $(NH_4)_2CrCl_4$.

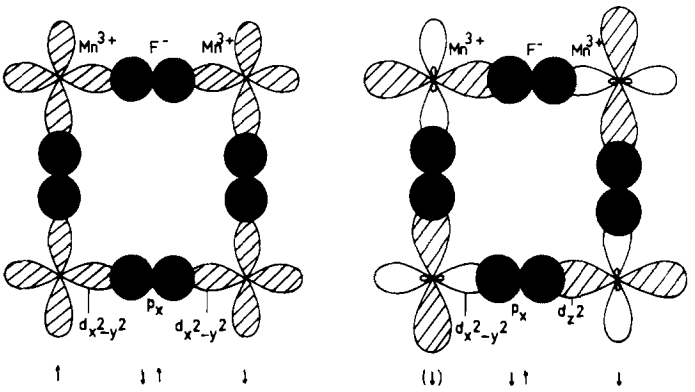

FIG. 15. Superexchange between d^4 cations via common corners in perovskite or perovskite-type layer structures. [*Left:* compressed octahedra; $d^1_{x^2-y^2} - d^1_{x^2-y^2} \rightarrow$ antiferromagnetism; *right:* elongated octahedra (anti-ferrodistortive order); $d^1_{z^2} - d^0_{x^2-y^2} \rightarrow$ ferromagnetism.]

discussed, they exhibit ferromagnetism at low temperatures (*24*). The ligand field spectra (Fig. 16) demonstrate that the d^4 cations Cr^{2+} and Mn^{3+} induce the same drastic distortion effects as Cu^{2+}. The E_g groundstate splitting is about 8000 cm^{-1} for Cr^{2+} and even 15,000 cm^{-1} for Mn^{3+} in the compounds considered.

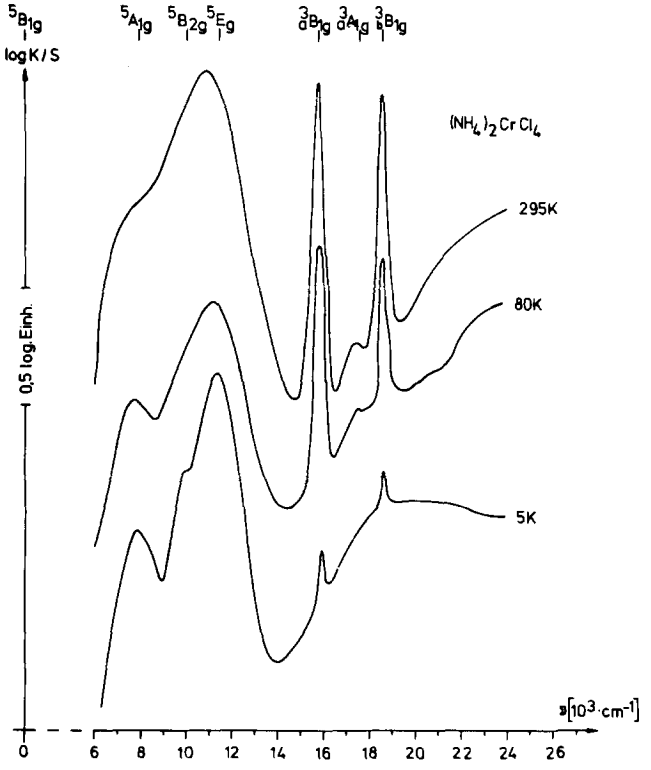

FIG. 16. Ligand field spectra of Cr^{2+} and Mn^{3+} in layer structures $A^I_2CrCl_4$ (*left*) and A^IMnF_4 (*right*).

4. Examples (Cu^{2+}, Ni^{3+})

In the following, we present two characteristic examples of Cu^{2+} compounds which illustrate how large the structural influence of a Jahn–Teller unstable cation may be in dependence on the geometry of the host-lattice structure. The perovskite and elpasolite structures with corner-linked octahedra are optimally adjustable to cooperative Jahn–Teller distortions. In Ba_2CuWO_6, for example, the CuO_6 octahedra exhibit differences between long and short CuO bond lengths of 0.44 Å and a ^2E_g ground-state splitting of 8600 cm^{-1} (*25*). Substituting W for Te changes the symmetry of connection between the octahedral sites (Fig. 17). Groups of three octahedra with common faces are connected by single octahedra via common corners (*26*). The sites occupied by Cu^{2+} are more rigid as the consequence of the geometric fixation by a common face and hence less adjustable to tetragonal distortion effects than in the elpasolite structure. The bond length differences within the CuO_6 polyhedra are indeed only about 0.14 Å, if one averages over the trigonal distortion component imposed on the octahedra by the host-lattice structure. The ground-state splitting, with

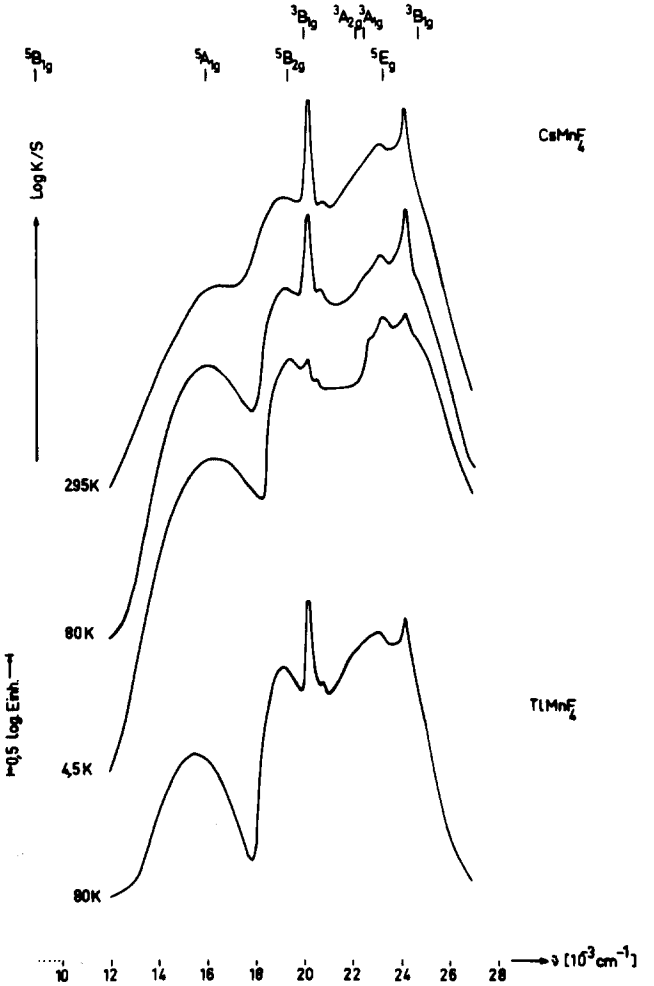

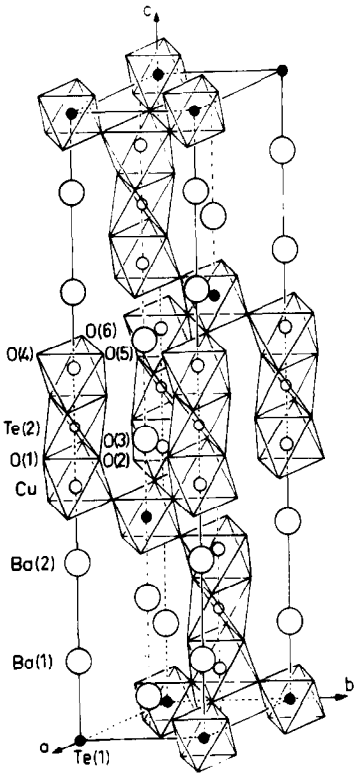

FIG. 17. The crystal structure of Ba_2CuTeO_6.

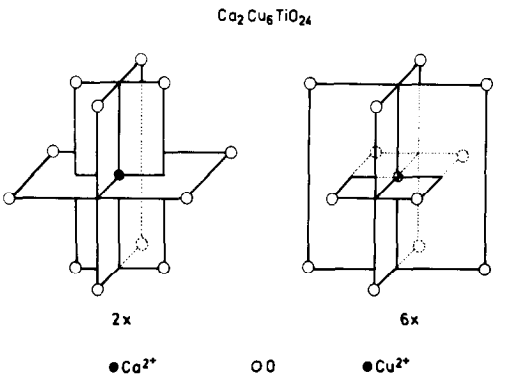

FIG. 18. The coordination polyhedra of Ca^{2+} and Cu^{2+} in $Ca_{1/4}Cu_{3/4}TiO_3$.

7600 cm^{-1}, is also smaller than the splittings for only corner-linked octahedra. Cu^{2+} ions may even completely change a host-lattice structure. It is possible to substitute exactly 75 mole% of Ca^{2+} by Cu^{2+} in the perovskite structure of $CaTiO_3$ (*27*) (Fig. 4), but hardly understandable that the small Cu^{2+} ion can be incorporated into a 12-coordinated site without appreciable displacements of the oxygen positional parameters. Indeed, the neutron diffraction results show that 75% of these sites are strongly distorted such that four oxygen ligands set up a square-planar coordination with Cu–O bond lengths of 1.95 Å, while the additional eight oxygen atoms are only very weakly bound (*28*) (Fig. 18). It is possible to retain this cubic structure type (space group $I2/m\bar{3}$), if the Ca^{2+} position is empty ($Cu_{3/4}Ti_{1/2}Ta_{1/2}O_3$), and even then, if the Cu^{2+} sites are partly unoccupied in addition (*28*). The last example refers to $CuTa_2O_6$, which crystallizes completely differently from $CuNb_2O_6$ and $CuSb_2O_6$.

In conclusion, we discuss some results concerning cations with a d^7 electronic configuration. It is well known that in elpasolite compounds $A^I_2B^IT^{III}F_6$ (A^I: Cs, Rb, K; B^I: Rb, K) the Co^{3+} ions in the T site possess a high-spin ground state, while the Ni^{3+} in these compounds is low-spin configurated (*29*). This behavior has not been well understood, because the crossover between the high-spin and low-spin configurations in octahedral coordination should occur at comparable ligand fields for related d^6 and d^7 cations, as is easily deduced from the Tanabe–Sugano diagrams. From the ligand field data and from the EPR spectroscopic g values of the Ni^{3+} elpasolites the energy level diagram of Fig. 19 could be calculated (*30*). From this diagram it follows that the high-spin configuration should indeed be more stable than the low-spin state in a *regular octahedral* coordination, in agreement with the isostructural Co^{3+} compounds (Fig. 19). The strong Jahn–Teller effect, however, leads to an appreciable splitting of the (excited) ^2E_g level, so that a low-spin ground state is finally stabilized. While the Jahn–Teller distortion of the $Ni^{III}F_6$ octahedra is dynamic at room

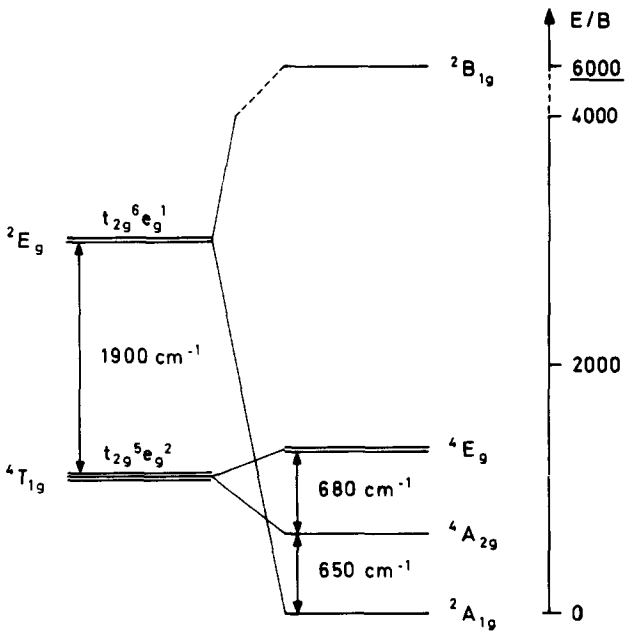

FIG. 19. Energy level diagram of Ni^{3+} in Cs_2KNiF_6. (*Left:* hypothetical O_h symmetry; *right:* D_{4h} symmetry.)

temperature, the tetragonal low-temperature modifications contain—as expected in analogy to Cu^{2+}—tetragonally elongated octahedra in ferrodistortive order (*30, 31*). The EPR spectrum of Cs_2NaNiF_6 is different from those reported above, because an isotropic high-spin signal of remarkable intensity is observed at about $g \approx 4$ in addition to the anisotropic low-spin signal (Fig. 20). This result can be understood from the crystal structure, which is analogous to that of Ba_2CuTeO_6 (Fig. 17). Half of the Ni^{3+} ions occupy the central octahedra of the groups, which are linked by common faces. They induce only relatively small Jahn–Teller effects, as was shown previously. Obviously the splitting of the ^2E_g state is not sufficiently large to stabilize the low-spin configuration. The second half of the Ni^{3+} ions occupy the octahedra, which are linked exclusively by common corners as in the elpasolite structure, so that a low-spin ground state is energetically favored. The conclusion extrapolated from this example is that the Jahn–Teller effect tends to stabilize the low-spin ground state of d^7 cations already at lower ligand fields than expected for a regular octahedral coordination (*30*).

Finally, we give some arguments concerning how to decide whether a distortion is caused by Jahn–Teller instability or by nonelectronic effects. A conclusive decision is possible for octahedral Cu^{2+}, for example, by comparing the Cu^{2+} compound in question with the stoichiometrically equivalent Ni^{2+} and Zn^{2+} compounds (Table II). Ni^{2+} and Zn^{2+} are similar to Cu^{2+} in electronic configuration and ionic size, but they have orbitally nondegenerate ground states in octahedral coordination. If the Cu^{2+} coordination is strongly distorted—in contrast to the Ni^{2+} or Zn^{2+} octahedra—the Jahn–Teller effect is very likely the energetic reason. Surely the Jahn–Teller effect is a stereochemically and energetically important factor in the structural chemistry of transition metal compounds.

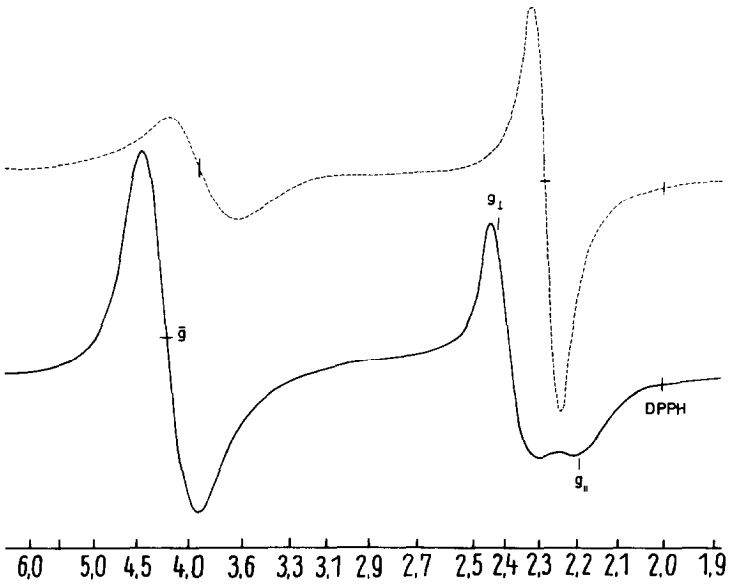

FIG. 20. EPR spectra of Cs_2NaNiF_6. – – –, 77°K; ——, 4.2°K.

TABLE II

BOND LENGTHS DATA (Å) AND CRYSTAL STRUCTURES OF Cu^{2+} COMPOUNDS COMPARED WITH THE CORRESPONDING Ni^{2+} COMPOUNDS

NiF_2 (Tetragonal)	1.98 (2×) 2.01 (4×)	CuF_2 (Monoclinic)	2.27 (2×) 1.93 (4×)	Rutile
$KNiF_3$ (Cubic)	2.00_5 (6×)	$KCuF_3$ (Tetragonal)	2.25 (2×) 1.96 (2×) 1.89 (2×)	Perovskite
K_2NiF_4 (Tetragonal)	1.97 (2×) 2.00 (4×)	K_2CuF_4 (Tetragonal)	2·22 (2×) 1·92 (4×)	
Ba_2NiWO_6 (Cubic)	~2.09 (6×)	Ba_2CuWO_6 (Tetragonal)	2.42 (2×) 1.98 (4×)	Elpasolite
$NiSb_2O_6$ (Tetragonal)	⟶	$CuSb_2O_6$ (Monoclinic)		Trirutile
$NiFe_2O_4$ (Cubic)	⟶	$CuFe_2O_4$ (Tetragonal)		Spinel

References

1. H. A. JAHN AND E. TELLER, *Proc. Roy. Soc., Ser. A* **161**, 220 (1937).
2. J. T. HOFF AND J. A. KONINGSTEIN, *Chem. Phys.* **1**, 232 (1972).
3. F. S. HAM, *in* "Electronic Paramagnetic Resonance" (S. Geschwind, Ed.), Plenum, New York (1972); A. ABRAGAM AND B. BLEANEY, "Electron Paramagnetic Resonance of Transition Ions," Oxford Univ. Press, pp. 790 ff. (Clarendon), London (1970).
4. C. FRIEBEL AND D. REINEN, *Z. Naturforsch. A* **24**, 1518 (1969).
5. H. O. WELLERN AND D. REINEN, unpublished results.
6. J. GREFER AND D. REINEN, Z. Naturforsch. A **28**, 464 (1973).
7. H. THOMAS, *in* "Anharmonic Lattices, Structural Transitions and Melting" (T. Rister, Ed.) Noordhoff, p. 213 Leiden, (1974).
8. D. REINEN AND C. FRIEBEL, "Structure Bonding," Springer-Verlag, Berlin/New York, in press.

9. A. OKAZAKI AND Y. SUEMUNE, *J. Phys. Soc. Japan* **16**, 176 (1961); **26**, 870 (1969).

10. J. A. BERTRAUD, D. A. CARPENTER, AND A. R. KALYANARAMAN, *Inorg. Chim. Acta* **5**, 113 (1970).

11. S. TAKAGI, M. D. JOESTEN, AND P. G. LENHERT, *Acta Crystallogr. B* **31**, 1970 (1975).

12. D. MULLEN, G. HEGER, AND D. REINEN, *Solid State Commun.* **17**, 1249 (1975).

13. D. REINEN, C. FRIEBEL, AND K. P. REETZ, *J. Solid State Chem.* **4**, 103 (1972); D. REINEN, *Solid State Commun.* **21**, 137 (1977).

14. G. BACKES AND D. REINEN, *Z. Anorg. Allg. Chem.* **418**, 217 (1975).

15. C. FRIEBEL, *Z. Anorg. Allg. Chem.* **417**, 197 (1975).

15a. S. KLEIN AND D. REINEN, *J. Solid State Chem.* **25**, 295 (1978); M. MORI, Y. NODA, AND Y. YAMADA, *Solid State Commun.* **27**, 735 (1978).

16. E. DUBLER, J. P. MATTHIEU, AND H. R. OSWALD, "Report, 4th Int. Conf. on Thermal Analysis, Budapest, 1974."

17. H. G. VON SCHNERING, *Z. Anorg. Allg. Chem.* **353**, 1, 13 (1967); **400**, 201 (1973).

18. D. REINEN AND H. WEITZEL, *Z. Naturforsch. B* **32**, 476 (1977).

19. D. BABEL AND R. HAEGELE, *Z. Anorg. Allg. Chem.* **409**, 11 (1974).

20. C. FRIEBEL AND D. REINEN, *Z. Anorg. Allg. Chem.* **407**, 193 (1974).

21. C. FRIEBEL, V. PROPACH, AND D. REINEN, *Z. Naturforsch. B* **31**, 109 (1976).

22. M. J. FAIR, A. K. GREGSON, P. DAY, AND M. T. HUTCHINGS, *in* "Proceedings, Int. Conf. of Magnetism, 1976," Part 2, p. 657 (1977).

23. P. KÖHLER AND D. REINEN, to be published.

24. P. KÖHLER, W. MASSA, D. REINEN B. HOFMANN, AND R. HOPPE, *Z. Anorg. Allg. Chem.*, in press.

25. D. REINEN AND H. WEITZEL, *Z. Anorg. Allg. Chem.* **424**, 31 (1976).

26. P. KÖHL AND D. REINEN, *Z. Anorg. Allg. Chem.* **409**, 257 (1974).

27. A. DESCHANVRES, B. RAVEAU, AND FR. TOLLEMER, *Bull. Soc. Chim. France*, 4077 (1967).

28. D. REINEN AND V. PROPACH, *Inorg. Nucl. Chem. Lett.* **7**, 569 (1971). V. PROPACH, *Z. Anorg. Allg. Chem.* **435**, 161 (1977).

29. W. KLEMM, B. BRANDT, AND R. HOPPE, *Z. Anorg. Allg. Chem.* **308**, 179 (1961); E. ALTER AND R. HOPPE, *Z. Anorg. Allg. Chem.* **405**, 167 (1974).

30. D. REINEN, C. FRIEBEL, AND V. PROPACH, Z. Anorg. Allg. Chem. **408**, 187 (1974).

31. J. M. DANCE, J. GRANNEC, AND A. TRESSAUD, *C.R. Acad. Sci.* **283**, 115 (1976).